Pergamon

Geochimica et Cosmochimica Acta, Vol. 68, No. 16, pp. 3339–3349, 2004

0016-7037/04 $30.00 + .00

doi:10.1016/j.gca.2003.10.013

Coprecipitation in the Barite Isostructural Family: 2. Numerical Simulations of Reactions and Mass Transport

CHEN ZHU*

Department of Geological Sciences, Indiana University, Bloomington, IN 47405-1405 USA

(*Received January* 13, 2003; *accepted in revised form October* 7, 2003)

Abstract—Coprecipitation of barite with trace constituents was simulated with consideration of aqueous speciation and complexation, mixing properties for the binary solid solutions (Zhu, this issue), precipitation and dissolution kinetics, and advective-dispersive transport. Speciation-solubility modeling was used to reproduce $BaSO_4$-$RaSO_4$ coprecipitation experimental results, and to calculate CrO_4^{2-} aqueous concentrations in equilibrium with a $Ba(SO_4,CrO_4)$ solid solution. Kinetic reaction path modeling was used to simulate the coprecipitation of barite with $RaSO_4$ to form an onion-like chemically zoned solid upon the cooling of oil field brine.

A one-dimensional coupled reactive mass transport model shows a strikingly different transport pattern for the tracer Ra^{2+}, when the dominant attenuation reaction is with solid solution (Ba, Ra) SO_4 as compared to the case when it is controlled by pure $RaSO_4$ and barite solids under local equilibrium conditions. A self-enrichment of Ra^{2+} in the groundwater and aquifer solid matrix—higher concentrations of Ra^{2+} downstream from the reaction front—results from the coprecipitation reaction and advective-dispersive transport. This self-enrichment process generates a secondary tracer source, which has tracer concentrations higher than that of the original source. On the other hand, coprecipitation reactions can reduce Ra^{2+} concentrations in groundwater to a much lower level (below ppb) than that of pure $RaSO_4$(c) solubility (near ppm), which has been used to establish the Ra^{2+} concentration limits in groundwater, soil, and nuclear waste repositories.

1. INTRODUCTION

Coprecipitation is a term commonly defined as the simultaneous removal of both tracer and carrier constituents from an aqueous solution, without regard to the specific mechanisms involved. Coprecipitation is important to cycling of trace element, sediment diagenesis, plaeoclimatology, formation of ore deposits, and to many environmental issues such as, acid mine drainage, potential radionuclide migration in fouled waste repositories, metal contaminant transport at industrial and defense sites, metal concentrations in aquatic systems, and wastewater treatment technology. While mechanisms of coprecipitation may vary in each case and may include surface adsorption, ion-exchange, surface precipitation, occlusion, and solid solutions, this paper deals with the formation and dissolution of solid solutions in the barite isostructural family.

The barite isostructural family minerals are important to both geological (see Hanor, 2000) and environmental processes. Ra^{2+} is commonly present in oil-field brines but at such low levels that the oil-field brines themselves do not pose a radiation safety risk, or precipitate pure $RaSO_4$ scale (Kraemer and Reid, 1984). However, Ra^{2+} is commonly coprecipitated in the barite scale (Smith, 1987; White, 1992; Gray, 1993; Fisher, 1995; National Research Council, 1999). The presence of ^{226}Ra and ^{228}Ra in the barite scale, even in trace amounts, generates radioactivity at a level of hundreds to thousands of pico-Curies per gram (pCi/g), greatly exceeding the 5 pCi/g safety standard (EPA, 1993). Thus, coprecipitation of Ra^{2+} with barite makes the barite scale a radioactive waste, commonly called Naturally Occurring Radioactive Material (NORM) or technology-enhanced NORM (TENORM).

Although the thermodynamic underpinning of coprecipitation has been long understood (McIntire, 1963; Stumm and Morgan, 1981; Morel, 1983; Sposito, 1984; Drever, 1988, 1992), coprecipitation reactions have been mostly described by partitioning coefficients, which is true for barite-$RaSO_4$ coprecipitation (Fisher, 1995) as well as for other important minerals (e.g., for calcite Curti, 1999). However, partitioning coefficients are phenomenological and empirical parameters. It is well known that partitioning coefficients are insufficient to describe the complex geochemical reactions (Reardon, 1981; Stumm and Morgan, 1996; Langmuir, 1997; Bethke and Brady, 2000; Zhu et al., 2001; Zhu and Anderson, 2002). In this study, the coprecipitation reactions were modeled within a thermodynamic and kinetic framework. The models include aqueous speciation and complexation, standard state and mixing thermodynamic properties of the solids and solid solutions, and precipitation and dissolution kinetics.

The transport patterns of contaminants when attenuated by coprecipitation reactions have not been thoroughly studied. Most reactive contaminant transport models simulate precipitation and dissolution reactions of pure solid phases in which the contaminant is the major component (Yeh and Tripathi, 1991; Walter et al., 1994a; Walter et al., 1994b). However, contaminant concentrations generally do not reach the levels of solubilities of their pure solid compounds. Only when the contaminant is a major constituent in groundwater, such as sulfate, do the dissolution and precipitation of pure phases form the dominant attenuation mechanism (Zhu and Burden, 2001; Zhu et al., 2001). In this study, a one-dimensional coupled

* Author to whom correspondence should be addressed (chenzhu@indiana.edu).

reactive transport model was used to simulate the dissolution-precipitation and reactive transport patterns when the contaminant of concern is a trace constituent of a major solid in an aquifer.

2. NUMERICAL COMPUTATIONS OF COPRECIPITATION REACTIONS

The thermodynamic formulation of coprecipitation reactions is given in Zhu (this issue). Note the formulation is equally applicable to anion or anionic group substitution, e.g., CrO_4^{2-} for SO_4^{2-}. In this case, the symbol of the binary solution may take the form of α(M, Tr), where α represents the remaining composition of the solid phase, e.g., Ba in solid solution Ba(SO_4^{2-}, CrO_4^{2-}), and *M* and *Tr* denote the major or carrier ion and tracer ion, respectively.

To model coprecipitation reactions, the geochemical equilibrium module EQMOD (Yeh, 1992) was expanded to include solid solutions. The mass action equations that describe the precipitation-dissolution of solid components can be rewritten as,

$$1 = \varphi_i^p \prod_{k=1}^{N} (C_k)^{a_{ik}^p} \quad i = 1, 2, \ldots, Mp \tag{1}$$

where C_k denotes the concentration of the *k*th aqueous component, superscript *p* is a precipitation-dissolution reaction, a_{ik} denotes the stoichiometric coefficients for the *k*th aqueous species in the *i*th reaction, *N* is the number of aqueous components in the model, and *Mp* is the number of precipitated components. φ is defined as,

$$\varphi_i^p = \frac{K_i^p}{a_i^p} \prod_{k=1}^{N} (\gamma_k)^{a_{ik}^p} \quad i = 1, 2, \ldots, Mp \tag{2}$$

where K_i is the equilibrium constant of the *i*th precipitation reaction, γ_k is the activity coefficient for the *k*th aqueous components, and a_i represents the activity of the *i*th solid.

Note that the activities for pure solids in the above equations are unity, as a result of the definition of the standard states of the solids as pure solids at the temperature and pressure of interest (see Section 3). Therefore, the precipitation and dissolution of pure solids are the degenerate cases in which the activity for the precipitated solid is unity.

To model coprecipitation reactions, Eqn. 1 is written for each end-member (e.g., $BaSO_4$ and $RaSO_4$). The residual function, *Re*, for the *i*th solid component, necessary for the Newton-Raphson method to solve the non-linear mass balance equations, can be written as

$$\mathrm{Re}(i) = 1 - \left[\varphi_i^p \prod_{k=1}^{N} (C_k)^{a_{ik}^p} \right] \quad i = 1, 2, \ldots, Mp \tag{3}$$

or, for the example of the $RaSO_4$ component in the (Ba, Ra)SO_4 solid solution, as

$$\mathrm{Re} = 1 - \left\lfloor K_{RaSO_4}^{barite} (\gamma_{Ba^{2+}} \gamma_{SO_4^{2-}}) (C_{Ba^{2+}SO_4^{2-}}) / X_{RaSO_4}^{barite} \lambda_{RaSO_4}^{barite} \right\rfloor \tag{4}$$

The Jacobian elements for the *i*th precipitated component (row) and *j*th aqueous component (column) are

Table 1. Solubility products* for barite structural family.

Species name	Formula	log *K*sp
barite	$BaSO_4$	−9.99[a]
	$RaSO_4$	−10.38[b]
hashemite	$BaCrO_4$	−9.76[c]

[a] Helgeson et al. (1978); [b] Sverjensky and Molling (1992); [c] Rai et al. (1988)
* at 25°C and 1 bar

$$J_{ij} = \frac{\partial \mathrm{Re}(i)}{\partial C_n} = \varphi_i^p \prod_{k=1}^{N} (a_{ik}^p) \frac{\partial (C_k)^{a_{ik}^p}}{\partial C_n} \quad n = 1, 2, \ldots, \mathrm{N}; \mathrm{j} = \mathrm{n} \tag{5}$$

When *j* represents a precipitated species, the Jacobian elements for the *j*th column when $i \neq j$ are,

$$J_{ij} = \varphi_i^p \prod_{k=1}^{N} (C_k)^{a_{ik}^p} X_i^p \frac{M_j^p}{(M_i^p)^2} \quad j = \mathrm{N} + \mathrm{Ns} + \mathrm{Mz} + n; \quad n = 1, \ldots, Mp \tag{6}$$

and when $i = j$,

$$J_{ij} = -\varphi_i^p \prod_{k=1}^{N} (C_k)^{a_{ik}^p} X_i^p \frac{1}{M_i^p} \quad j = \mathrm{N} + \mathrm{Ns} + \mathrm{Mz} + n; \quad n = 1, 2, \ldots, Mp \tag{7}$$

where M_i^P denotes mol/L of the *i*th solid component, M_j^P represents moles of the *j*th solid component, and *Ns* and *Mz* represent the number of adsorbed component and ion-exchanged species, respectively.

The modified code, EQMODCP, was verified against hand-calculations and calculations from EQ3 (Wolery, 1992) for the cases of ideal solid solution (Ca, Mg)CO_3, regular solid solution (Ba, Ra)SO_4, and subregular solid solution (Fe^{3+}, Cr^{3+})$(OH)_3$. The results from EQMODCP compare well with those from EQ3. These results further compare well to those from the code PHREEQC (Parkhurst and Appello, 1999). Recently, solid-solution aqueous solution reactions are also modeled using the Gibbs free energy minimization method (Kulik et al., 2000). However, we are unable to make comparisons to that approach at the present time.

3. STANDARD STATES AND THERMODYNAMIC PROPERTIES

The standard states for the solid solution end-members $BaSO_4$, $RaSO_4$, and $BaCrO_4$ are defined as unit activity for pure end-member component at the temperature and pressure of interest. The standard state for water is unit activity of pure water; for aqueous species other than H_2O, the standard state is unit activity of the species in a hypothetical one molal ideal solution referenced to infinite dilution at the temperature and pressure of interest. The standard states for pure solids are unit activities at the temperature and pressure of interest.

Table 2. Association constants at 25°C and 1 bar for aqueous complexes of interest in this study.

Aqueous complex	log K
$Ra^{2+} + Cl^- = RaCl^+$	−0.10[a]
$Ra^{2+} + 2Cl^- = RaCl_2^o$ (aq)	−0.05[b]
$Ra^{2+} + SO_4^{2-} = RaSO_4^o$ (aq)	2.76[a]
$Ba^{2+} + Cl^- = BaCl^+$	−0.50[c]
$Ba^{2+} + SO_4^{2-} = BaSO_4^o$ (aq)	2.7[d]
$Ba^{2+} + OH^- = BaOH^+$	−0.24[e]
$Ba^{2+} + CO_3^{2-} = BaCO_3^o$ (aq)	2.71[d]
$Sr^{2+} + OH^- = SrOH^+$	−13.29[d]
$Sr^{2+} + SO_4^{2-} = SrSO_4^o$ (aq)	2.29[d]
$Sr^{2+} + Cl^- = SrCl^+$	−0.25[c]
$Sr^{2+} + CO_3^{2-} = SrCO_3^o$ (aq)	2.81[d]
$CrO_4^{2-} + H^+ = HCrO_4^-$	−6.52[f]
$Sr^{2+} + HCO_3^- = SrHCO_3^-$	1.18[d]

[a] Langmuir and Riese (1985); [b] Phillips (1988); [c] Sverjensky et al. (1997); [d] Nordstrom et al. (1990); [e] Glushko et al. (1979); [f] Shock et al. (1997).
* at 25°C and 1 bar

Solubility products for end-members in the barite isostructural family used in the simulations below are listed in Table 1. For modeling aqueous speciation, thermodynamic properties for the Ra^{2+} and Ba^{2+} aqueous species are needed. However, there are few experimental data available for the aqueous Ra^{2+} species; most of the thermodynamic properties in recent reviews and compilations are estimates (Langmuir and Riese, 1985; Lawson, 1985; Phillips et al., 1988). The association constants for Ba^{2+} and Ra^{2+} complexes used in the speciation simulation are listed in Table 2. For all other ions and complexes not listed, constants were calculated using thermodynamic data from Shock and Helgeson (1988), Shock et al. (1997), and Sverjensky et al. (1997). Temperature dependence of the log K for aqueous species and pure solid was either calculated from the Van't Hoff equation or the analytical expression embedded in PHREEQC.

Mixing properties of the binary solid solutions, (Ba, Ra)SO_4 and Ba(SO_4, CrO_4), are from Zhu (this issue). Rational activity coefficients for solid solution end-members were calculated at different temperatures assuming the Margules parameters are constant over the temperature range of interests (25 to 100°) Activity coefficients for charged aqueous species were calculated from the WATEQ extended Debye-Hückel equation fitted to mean salt NaCl activity coefficients (Truesdell and Jones, 1974). For neutral species, the activity coefficients were assumed to be unity.

4. SIMULATION OF CONTAMINANT TRANSPORT WITH COPRECIPITATION REACTIONS

4.1. Reproducing Coprecipitation Experiments

The experiments on $BaSO_4$-$RaSO_4$ coprecipitation carried out by Doerner and Hoskins (1925) are best known for the Doerner and Hoskins Logarithm Distribution Law, which describes, empirically, the local equilibrium distribution of the tracer between a zoned solid (the "onion") and a solution in a closed system that allows free drifting of solution chemistry while precipitation takes place. However, they also conducted coprecipitation experiments in which sulfuric acid was added into $RaCl_2$-$BaCl_2$ solutions while the solution was being agitated and the crystals were digested between each addition. They believed that the results obtained using this method represent the equilibrium distribution of Ra^{2+} between homogeneous solids and aqueous solutions and were due to repeated dissolution and recrystallization. These experiments allow us to compare results from our simulation with the experimental results.

Figure 1a,b shows that the simulated moles of Ra^{2+} coprecipitated with $BaSO_4$ agree with experimental results. Such close agreement is remarkable, since the thermodynamic model described in Zhu (this issue) is independent of these experimental results. Figure 1c,d shows the aqueous speciation of Ba^{2+} and Ra^{2+} in the four different experimental sets. The conditional nature of partitioning coefficients is shown as being influenced by aqueous complexation. Figure 1e shows the partitioning coefficients

$$K_D = \frac{(X_{RaSO_4}/X_{BaSO_4})}{(m_{Ra^{2+}}/m_{Ba^{2+}})}$$

and

$$K_{D'} = \frac{(X_{RaSO_4}/X_{BaSO_4})}{(m_{t,Ra^{2+}}/m_{t,Ba^{2+}})}$$

as a function of total chloride concentration, where m_t is the total dissolved aqueous concentration. The above simulation results from EQMODCP also match well with the simulation results using EQ3NR and PHREEQC when the same equilibrium constants are used for all programs.

4.2. Coprecipitation of Barite and $BaCrO_4$

$BaCrO_4$ has a barite-like structure, and unlike $RaSO_4$, its solubility is only slightly higher than that of barite (Table 1). The effectiveness of coprecipitation reactions in control of trace constituents, when the solubilities of the tracer and carrier are similar, is explored with modeling of Ba(SO_4, CrO_4) coprecipitation. Here, the total CrO_4^{2-} concentrations in an aqueous solution at equilibrium with a Ba(SO_4, CrO_4) binary solid solution were calculated. A Margules parameter, W, value of 257 cal/mol from Zhu (this issue) was used to calculate the activity coefficients for $BaSO_4$ and $BaCrO_4$ end-members. The equilibrium constants for aqueous species are listed in Table 2. In the simulation, the aqueous solution initially has 0.2 mmol/L of barium and sulfate, a pH of 5, and a range of Cr(VI) concentrations.

As expected, the total aqueous CrO_4^{2-} concentrations increase with increasing mole fractions of $BaCrO_4$ (Fig. 2). The dominant aqueous Cr(VI) species is $HCrO_4^-$. The solid solution maintains the CrO_4^{2-} at about 1 ppm in the aqueous solution. However, the U.S. EPA Maximum Concentration Limit (MCL) for drinking water standard is 0.1 ppm. Thus, coprecipitation of two end-members with similar solubility does not maintain the tracer at a low concentration level.

4.3. Precipitation of Mixed Scale from Oil Field Brine

This case simulates NORM scale formation when oil field brine at 100°C is brought up to ground surface and cooled to

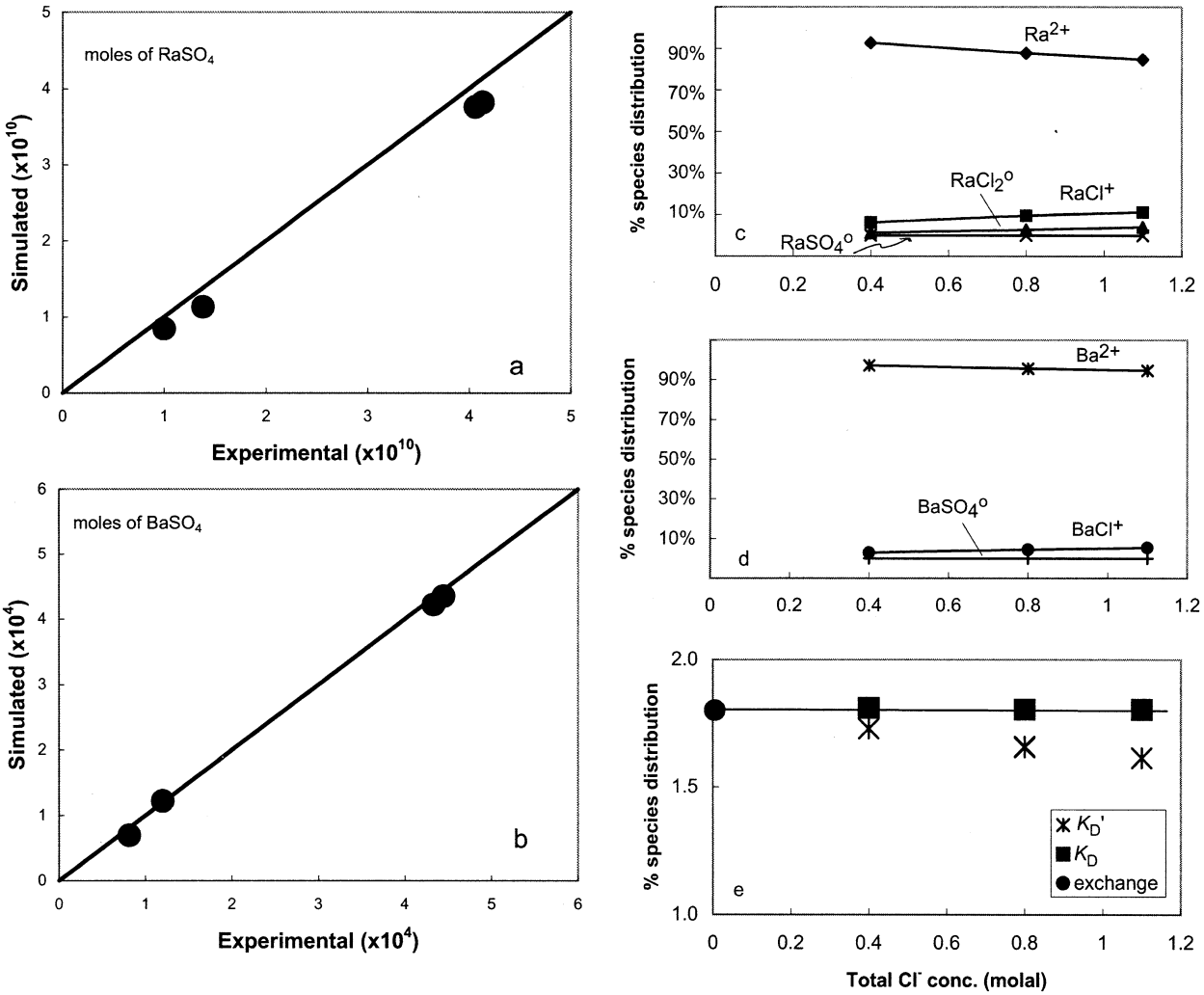

Fig. 1. Comparison of experimental results with model simulations. Experimental data for (Ba, Ra)SO_4 coprecipitation is from Doener and Hoskins (1925), (a) moles of $RaSO_4$ coprecipitated; (b) moles of $BaSO_4$ coprecipitated; (c) and (d) aqueous species distribution for Ra^{2+} and Ba^{2+}; and (e) calculated partitioning coefficients. The "exchange" symbol represents the Ra-Ba exchange reactions in dilute HCl solution.

25°C. During the enhanced oil recovery processes, barite scale is commonly formed at the surface (in wellheads, tubes, equipment, and tanks) due to a decrease in temperature. Geochemical modeling of coprecipitation can lead to a better anticipation of NORM scale formation. However, previous modeling work has mostly used distribution coefficients to calculate radium in the barite scale (Fisher, 1995), which implicitly assumed homogeneous solids. As is shown in Figure 1, K_D is empirical and a function of aqueous speciation, among other factors. The availability of mixing properties for the $BaSO_4$-$RaSO_4$ binary (Zhu, this issue) allows the coprecipitation of (Ba, Ra)SO_4 to be modeled with a thermodynamics framework, together with precipitation-dissolution kinetics.

The composition of the simulated brine is listed in Table 3. The brine contains 100 parts per trillion (ppt) radium. In this study, homogenous reactions, i.e., aqueous complex formation and dissociation, are treated as equilibrium reactions. The precipitation and dissolution reactions are simulated as a kinetic process and are described with the following rate law (Dove and Czank, 1995),

$$Rate = S_A k_+ (1 - \Omega) \tag{8}$$

where *Rate* stands for the reaction rate for the reactant (mol L^{-1} s^{-1}), S_A denotes the surface area (m^2/L), and *k* denotes the rate constant (mol m^2 s^{-1}) defined as,

$$k_i = Ae^{\frac{-Ea}{RT}} \tag{9}$$

where *A* stands for the Arrhenius preexponential factor (mol m^2 s^{-1}), and E_a represents the activation energy (J/mol). Values of *E*a and *A* were regressed from experimental data at about pH 5.7 (Dove and Czank, 1995). Ω represents the saturation quotient (Q/K), and the term (1-Ω) forces the total rates to approach zero as equilibrium is approached. The term also takes into account both supersaturation [(1-Ω) > 1, overall rate >0]

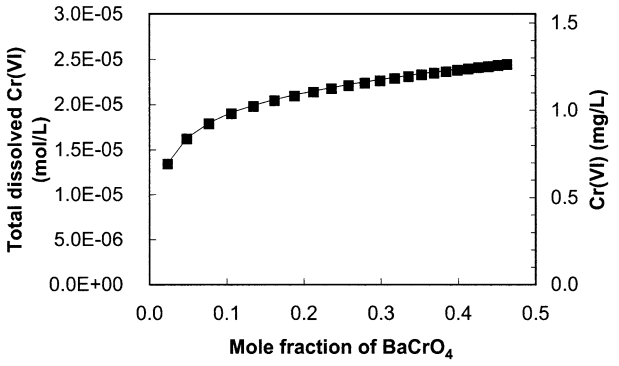

Fig. 2. Concentrations of total dissolved CrO_4^{2-} in an aqueous solution at equilibrium with the $Ba(SO_4, CrO_4)$ solid solution.

and under-saturation [$(1\text{-}\Omega) < 1$, overall rate <0]. However, whether the form of Eqn. (8) is suitable for modeling precipitation reactions is questionable. In general, we know very little about the proper form of rate laws for precipitation reactions in geochemistry (Lasaga, 1998).

Although solid solutions show different dissolution rates from the end-members (see review by Dove and Czank, 1995), the $RaSO_4$ mole fraction is so small in this study that the kinetic rate for barite should be an adequate approximation. Thus, computationally, barite precipitation is modeled according to the kinetic law expressed above, but the $RaSO_4$(s) component is incorporated into barite by equilibrium fractionation according to the regular solid solution model given in Zhu (this issue).

For simulations in this study, the geometric surface areas were calculated by assuming barite grains to be 0.01 mm cubes. Surface roughness, which is commonly considered in dissolution kinetics and can vary over a factor of 10 to 2000 (White and Peterson, 1990), was neglected. It has been argued that the geometric surface area is equal to the effective reactive surface area in dissolution experiments (see Gautier et al., 2001). Murphy and Helgeson (1988) found that the effective reactive surface areas can be orders-of-magnitude lower than the total surface area. However, the subject of reactive surface areas is poorly understood in kinetic studies, and particularly so for precipitation reactions (see Rimstidt and Barnes, 1980). Thus, for the sake of simulation, an initial "seed" surface area equivalent to barite concentration of 4.2×10^{-5} mol/L was used.

It is well known that, as a crystal grows from the aqueous solution, it becomes increasingly difficult to maintain equilibrium between the interior of the crystal and the aqueous phase (Doerner and Hoskins, 1925). This is due to the slow diffusion of ions through solids at low temperatures. In the model, we "sequestrated" the precipitated solid solutions from further reactions after each reaction step (see Wolery, 1992 on computational methods for pure solids, but here is for solid solution). This computational scheme attempts to mimic the following conceptual model; as the outmost surface of the crystal is formed, $RaSO_4$ is at equilibrium with the aqueous solution of that time. However, this surface layer is covered up by the succeeding layer (of the next reaction step) and does not re-equilibrate with the aqueous phase despite the difference in chemical potential between this layer and the aqueous solution. As a result, the solid solution compositions vary from the center of the crystal outward, forming a Doerner and Hoskins type, layered or "onion" zoning.

Murphy and Smith (1988) developed a model for irreversible dissolution of an ideal solid solution. In their model, the dissolution is stoichiometric with respect to the original solid solution composition, but the reverse reaction precipitates a solid solution on the solid surface with a different stoichiometry, corresponding to the solid solution composition with the greatest affinity to precipitate. With the asymmetry stoichiometry in the dissolution and growth reactions, Murphy and Smith (1988) were able to simulate time-variable chemical compositions on mineral surfaces. At the present time, we are unable to make comparison to this approach.

In our simulation, the brine was allowed to cool from 100 to 25°C over five days. During this period, barite was precipitated. The precipitation of barite correlated with a reduction of Ba^{2+} concentration in the brine (Fig. 3b). The majority of Ba^{2+} precipitated out within the first two days. The continued precipitation of a small amount of barite (Fig. 3b,f), after $\sim$ 2.5 d, and the more pronounced changes in Ba^{2+} aqueous concentrations is an artifact of the computation scheme. Ra^{2+} was coprecipitated with barite (Fig. 3c), despite the fact that the brine was undersaturated with respect to pure $RaSO_4$(c) solid (Fig. 3c, vertical axis on the right). The reduced solubility came from a mole fraction of about 10^{-5} to 10^{-8} for the $RaSO_4$ end-member (Fig. 3c). A large percentage of Ra^{2+} was rapidly coprecipitated from the brine (Fig. 3e), consistent with our knowledge of preferential partition of Ra^{2+} into the barite with respect to aqueous solution. The coprecipitation (fractionation) process concentrated the Ra^{2+} from ppb levels in the oil-field brine to ppm in the barite scale (Fig. 3e).

The rate of barite precipitation is shown in Figure 3d. Rates decrease sharply as the solution approaches equilibrium with barite (see Eqn. 8). The amount of barite and $RaSO_4$(s) precipitated at each time step is shown in Figure 3f.

Figure 3c shows the mole fraction of $RaSO_4$(s) in barite, which decreases as reaction proceeds. These mole fractions represent the composition of the solid solution precipitated at each time step. These results demonstrate that an "onion" like

Table 3. Compositions of the oil field brine used in the simulation.

Elements	Conc. (mg/L)
Na	11,000
K	250
Ca	800
Mg	150
Sr	75
Ba	25
Cl	19,000
Ra	100 ppt*
SO_4^{2-}	300
HCO_3^-	300
pH	6
Temp (°C)	100

* parts per trillion

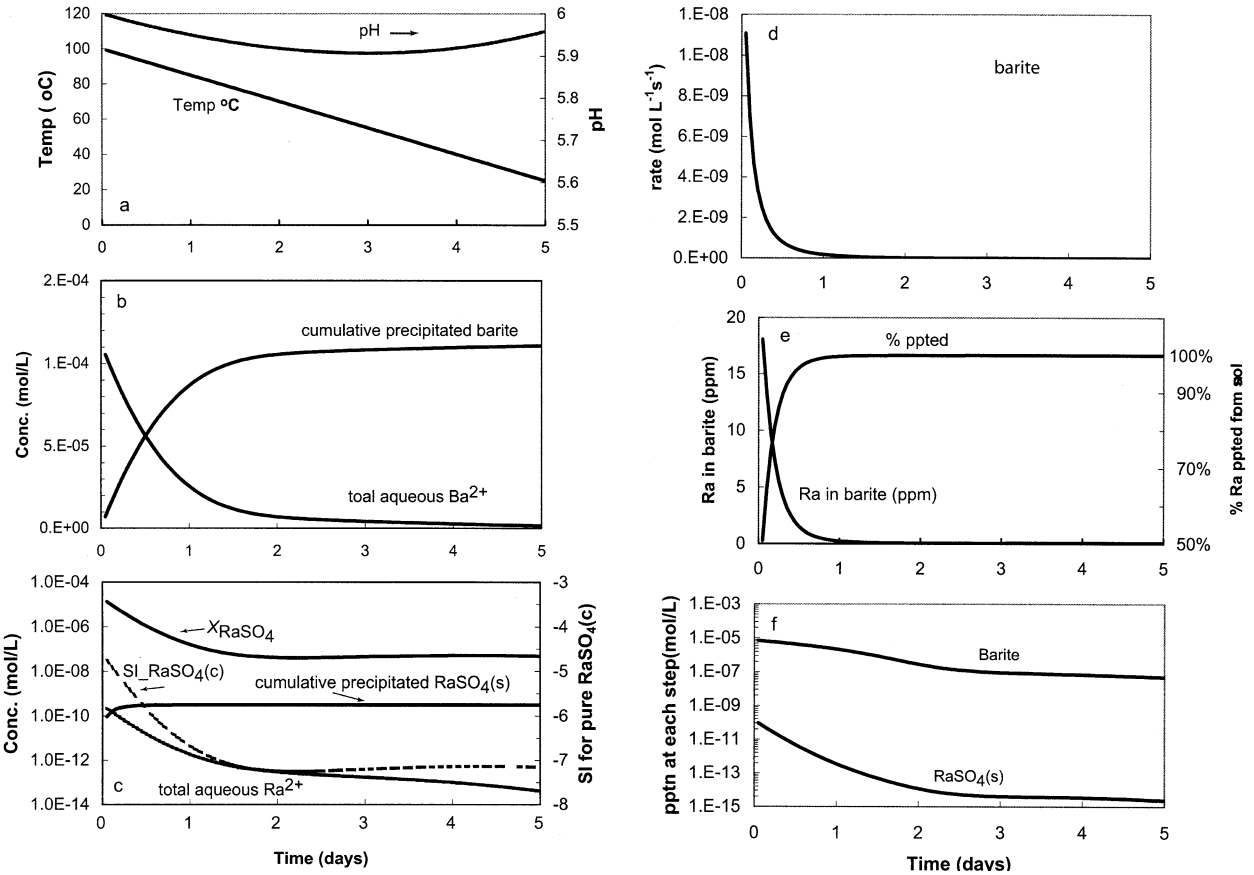

Fig. 3. Kinetics reaction path modeling of precipitation of radioactive barite scale during cooling of an oil field brine from 100 to 25°C. Note that the amounts of precipitated barite and $RaSO_4$ are for total accumulated in the system in (b) and (c), but for each reaction step (ΔT = 0.75 °C, Δt = 0.05 d) in (f). The mole fraction, X_{RaSO_4}, in (c) is also for each reaction step so that the model predicted an "onion" type layered solid precipitate.

zoning on precipitated solids is predicted from this kinetic model in this study.

4.4. Dissolution/Coprecipitation of (Ba, Ra)SO_4 in Flowing Groundwater

There are tremendous interests in the leaching of (Ba, Ra)SO_4 sludges, produced from uranium mining and milling and oil and gas production, in groundwater (see Huck et al., 1989 and refs therein). The example of (Ba, Ra)SO_4 leaching and Ra^{2+} transport in groundwater aquifers below also bears significance and generality to understanding trace element mobility and distribution in geological media when coprecipitation reactions are the dominant reactions controlling trace element solubility and mobility.

This computational problem mimics a groundwater aquifer with buried NORM as the contaminant source. The one-dimensional spatial domain is divided into 10 cells, each 1-m in length. Cauchy boundary conditions are set at both ends of the column. The incoming fluid is nearly pure water and hence undersaturated with respect to the solid solution. Dispersivity is assumed to be 0.1 m or one-tenth of the length of the domain. A uniform and constant Darcy velocity of 5 m/yr and a time step of 0.2 yr for a total of 10 yr were specified. Molecular diffusion was neglected in the model.

A total of six aqueous components—H^+, Cl^-, SO_4^{2-}, Na^+, Ba^{2+}, Ra^{2+}—and one mineral solid solution—(Ra, Ba)SO_4—are included in the model. Aqueous speciation is calculated using the equilibrium constants listed in Table 2. The solid solution is allowed to dissolve and precipitate according to its saturation state with respect to the aqueous solution chemistry. The background electrolyte solution is a 0.01 molal NaCl solution. All chemical reactions are calculated at 25°C and 1 bar. Initial pore fluid composition is controlled by equilibrium with the (Ba, Ra)SO_4 solid solution with a trace amount of $RaSO_4$(s) (8.41×10^{-7} mol/L). The local equilibrium assumption (LEA) is used.

The advection, dispersion, and reaction of the six components under the above initial and boundary conditions were simulated by using PHREEQC Version 2.0 (Parkhurst and Appello, 1999), a one-dimensional finite-difference code. The advection-dispersion-reaction (ADR) equation,

$$\frac{\partial C}{\partial t} = D_L \frac{\partial^2 C}{\partial \chi^2} - \bar{v}\frac{\partial C}{\partial \chi} - \frac{\rho_b}{\theta}\frac{\partial S}{\partial t} \tag{10}$$

was solved, where C and S represent concentrations in fluid and

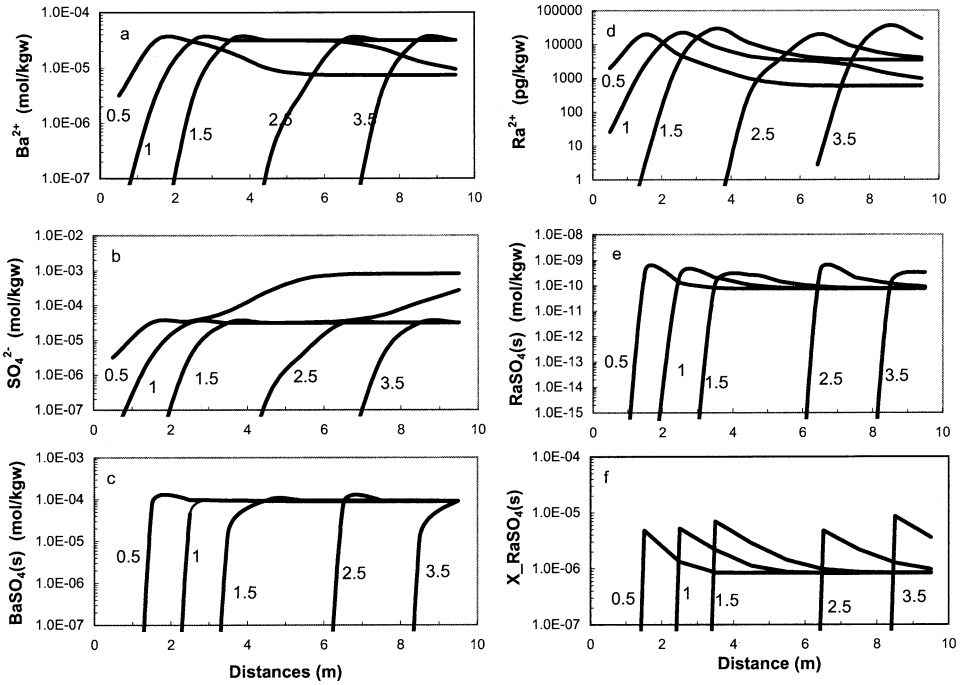

Fig. 4. Concentration profiles at 0.5, 1, 1.5, 2.5 and 3.5 pore volumes of influent.

solid matrix, respectively, t denotes time (T), x is distance (L), ρ_b is the bulk density of the aquifer (M/L^3), and θ is the effective porosity. $\bar{v}$ denotes the average linear velocity of groundwater (M/L), and D_L is the longitudinal hydrodynamic dispersion coefficient (L^2/T) as described by Bear (1972)

$$D_L = \bar{v}\alpha_L + D^o\tau \tag{11}$$

where α_L stands for longitudinal dispersivity (L). D^o and τ represent the molecular diffusion coefficient (L^2/T) and tortuosity (dimensionless), respectively. The reaction term, $\frac{\rho_b}{\theta}\frac{\partial S}{\partial t}$, is solved separately for each cell using a chemical module in which chemical speciation and partitioning between the solid matrix and aqueous solutions are calculated based on the mass-balance and mass-action equations (see Parkhurst, 1995).

In PHREEQC, a split-operator scheme is used to solve the advective and dispersive transport at consecutive stages. Within each time step, the advective transport is calculated first using an upwind finite difference scheme. This is followed immediately by a calculation of chemical reactions. Dispersive transport is then calculated using a central difference scheme (or mixing cell method). This is again followed by a calculation of chemical reactions. No iterations between the physical and chemical steps are used (cf. Yeh and Tripathi, 1989).

As expected, the results show Ra^{2+} is favorably partitioned into barite with respect to the aqueous phase (Fig. 4). Dissolved Ra^{2+} is scavenged into the solid solution downstream. Hence, the mole fraction of $RaSO_4$(s) immediately downstream from the dissolution front is an order of magnitude higher than the initial solid composition. Correspondingly, the groundwater that is at equilibrium with this high $RaSO_4$ mole fraction (Ba, Ra)SO_4 solid solution has aqueous Ra^{2+} concentrations more than an order of magnitude higher than the initial equilibrium concentrations.

In contrast, the SO_4^{2-} and Ba^{2+} concentrations do not show a significant increase downstream from the dissolution front because the mole fraction changes for the barite end-member component are minimal. In the model, the equilibrium aqueous concentrations of Ba^{2+} and SO_4^{2-} are reset initially when incoming fluid dissolves the solid solution and mass transfer from the solid to the solution takes place. This results in an increase of Ba^{2+}, but this increase is coherent with a decrease of SO_4^{2-} concentration. The activity product of SO_4^{2-} and Ba^{2+} remains the same because the fluid maintains equilibrium with the solid solution. Barium and sulfate concentrations reach a new plateau after one pore volume in the region where the solid solution phase is present.

The self-enrichment transport pattern of the tracer is also illustrated in the breakthrough curves in the fifth cell (Fig. 5). There are several waves shown in the breakthrough curves. Helfferich (1989) defined “wave” (synonymous with “front”) as any variation of solute or solid phase concentration. Radium is initially controlled by equilibrium with the solid solution specified in the initial condition. This is manifested as a concentration plateau from 0 to 0.5 of the pore volume. However, from there, Ra^{2+} concentrations gradually increase to more than one order of magnitude over the initial concentration, corresponding to the increase of mole fraction (Fig. 4d).

By comparison, the structure of the breakthrough curves for the major constituents SO_4^{2-} or Ba^{2+} are different. The concentration-plateaus for Ba^{2+} and SO_4^{2-} initially correspond to the pore fluids and solid solution compositions specified in the initial condition. At about 0.5 pore volume, an advective-

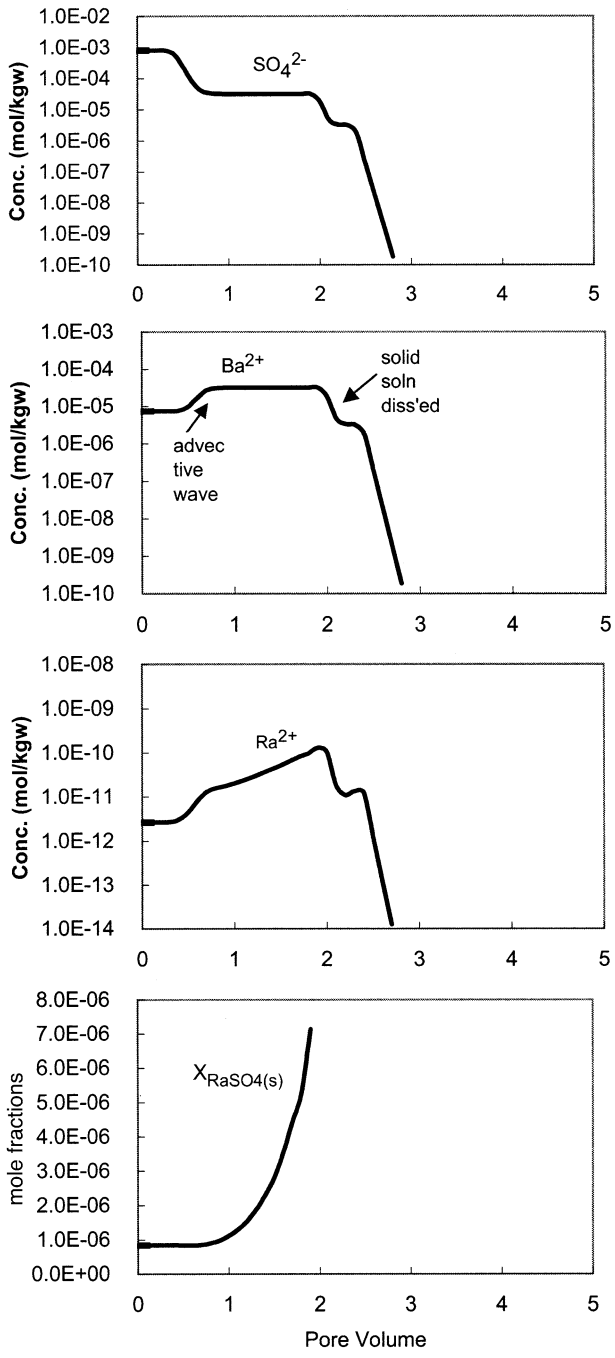

Fig. 5. Break-through curves at the fifth cell of the model.

dispersive wave of higher barium (and correspondingly lower SO_4^{2-}) concentrations arrived. The activity product of SO_4^{2-} and Ba^{2+} remains the same because the solution is at equilibrium with the solid solution. Barium and sulfate concentrations have a higher or lower plateau controlled by the equilibrium with the solid solution in which barite mole fraction and activity is close to one. However, the Ba^{2+} concentrations do not increase with time as the Ra^{2+} concentration does. At about 2 pore volumes, all the solid solution is dissolved and the concentrations for Ba^{2+} and SO_4^{2-} drop drastically. At about 2.5 pore volumes, SO_4^{2-}, Ba^{2+}, and Ra^{2+} concentrations are reduced to zero because the incoming fluid contains none.

These computational results illustrate a mechanism of secondary enrichment of the contaminant in downstream areas if coprecipitation is the dominant reaction and local equilibrium is attained. The different transport patterns when solute is controlled by the solubility of a pure solid and a solid solution are further illustrated in Figure 6. In this simulation, all initial and boundary conditions are the same as those described in the model above. The only difference is that a pure $RaSO_4$(c) phase and pure barite, rather than a solid solution, are at equilibrium. The results show that Ra^{2+} concentrations do not increase with time. There is also no secondary enrichment in the aquifer solid matrix (Fig. 6e). The breakthrough curves in the fifth cell for the pure barite and $RaSO_4$ (c) case are plotted in Figure 7. They also demonstrate no secondary enrichment.

Additionally, the calculations show that $RaSO_4$ as the tracer in the (Ra, Ba)SO_4 solid solution controls Ra^{2+} concentrations in groundwater in parts per trillion to parts per billion (Fig. 5). However, if controlled by the pure $RaSO_4$ (c) phase, Ra^{2+} concentrations are nearly at a parts-per-million level (Fig. 6). Previous studies that did not consider coprecipitation or solid-solution, yielded unrealistically high concentrations (0.1 ppm) in groundwater and soil (Lindsay, 1988) and in high-level nuclear waste repositories (Nagra, 1994).

5. CONCLUSIONS

This study has modeled the coprecipitation reaction within a thermodynamics and kinetics framework. The model for coprecipitation of (Ba, Ra)(SO_4) and Ba(SO_4, CrO_4) binary solid solutions includes aqueous speciation and complexation, standard state and mixing thermodynamic properties of the solids and solid solutions, precipitation and dissolution kinetics, and advective-dispersive mass transport. Numerical simulations show quantitatively that (1) a tracer component in a solid solution can reduce the solubility of this tracer in aqueous solutions, particularly when the tracer component has a lower solubility than the carrier; and (2) under local equilibrium conditions, the interactions between solid solutions and a flowing fluid result in a self-enrichment process, through which trace elements in geological fluids can be greatly enriched in host minerals.

However, coprecipitation reactions are complex, and our models are simplistic at best. Equilibrium between solid solutions-aqueous solutions is often not achieved in low-temperature systems (e.g., Plummer, 1986). The coprecipitated solids also may be first amorphous and, with time, change to more crystalline forms (Ostwald ripening, see Steefel and Van Cappellen, 1990; Lasaga, 1998). In geochemistry, many fundamental questions about dissolution and precipitation kinetics remain unanswered, particularly for precipitation reactions, e.g., the “reactive surface area,” reaction mechanisms, and proper rate laws. Many different mechanisms may be involved in coprecipitation, in addition to solid solution formation (see Introduction).

Although our example is at low temperature and mostly directed at environmental impacts, this approach of thermodynamics-kinetics modeling will find abundant, and perhaps better, applications to ore deposits (Holland, 1956; Barnes and Kullerud,

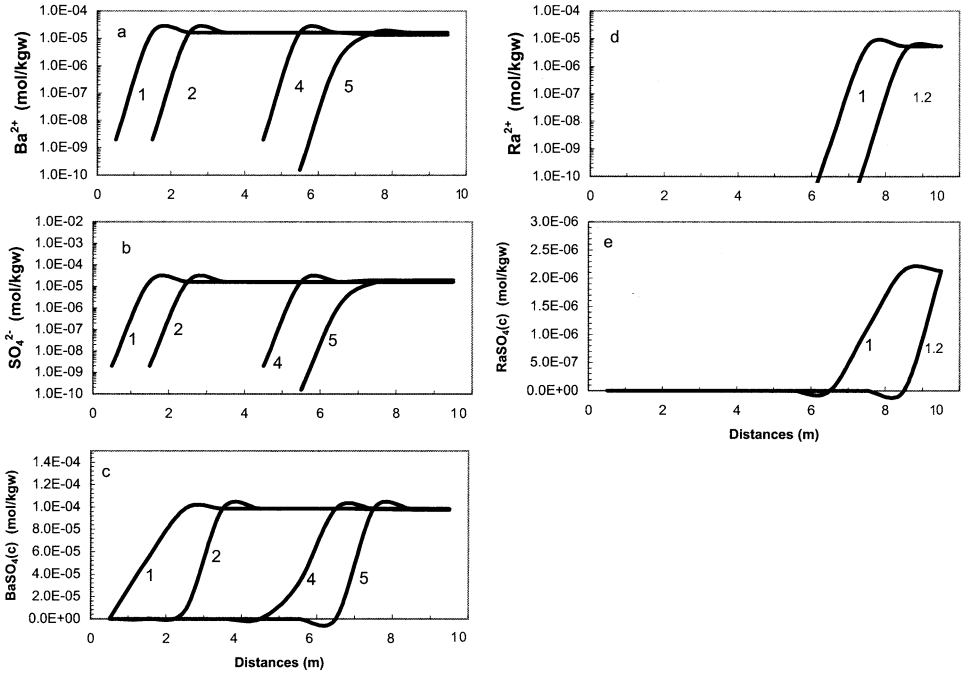

Fig. 6. Concentration profiles for the case of precipitation and dissolution of pure $RaSO_4$ and $BaSO_4$ phase. Numerical figures on the curves are pore volumes.

1957), hydrothermal systems, and metamorphic petrology. Moreover, new high-resolution electron microscopic techniques now permit subnanometer scale images and nanometer scale quantitative chemical analyses (Zhu et al., 1994; Penn et al., 2001). The thermodynamics and kinetics models presented here, when combined with high resolution chemical zoning data, will no doubt greatly advance our understanding of the coprecipitation mechanisms and chemical evolution of geological fluids.

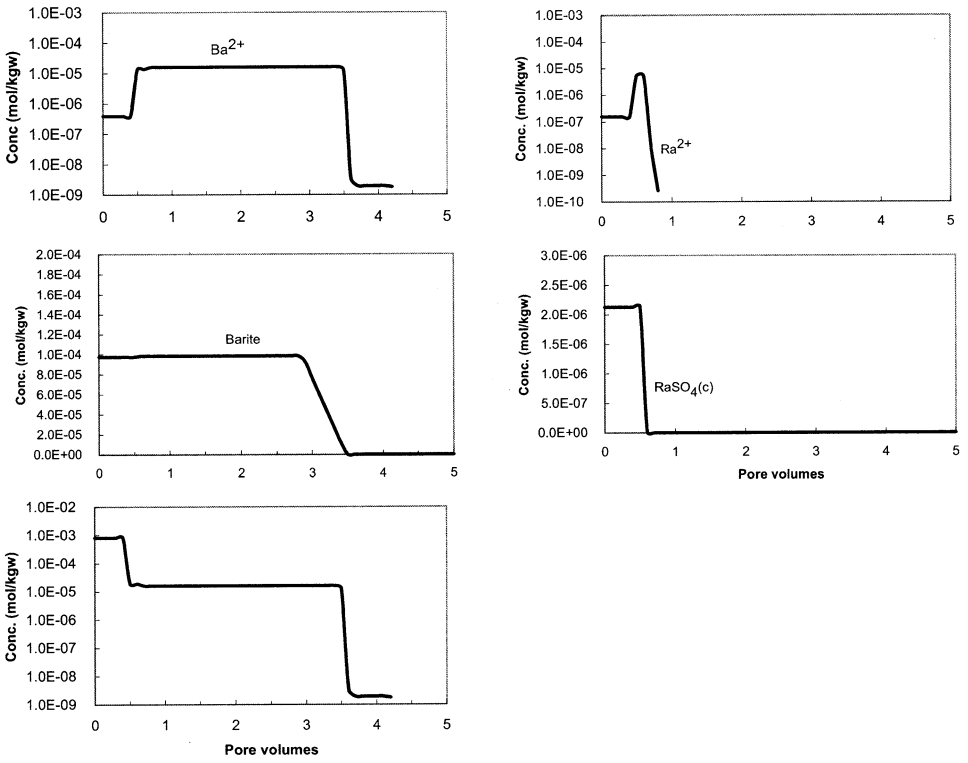

Fig. 7. Break-through curves at the fifth cell of the model of pure barite and $RaSO_4$(c).

Acknowledgments—The author is grateful to Bill Murphy, Don Rimstidt, and two anonymous reviewers, whose review comments greatly helped to improve the paper. Thanks are also due to David Parkhurst who helped to devise a strategy to simulate kinetic precipitation of a solid solution using PHRQEEC.

Associate editor: J. D. Rimstidt

REFERENCES

Barnes H. L. and Kullerud G. (1957) Relations between composition of ore minerals and ore solutions. *Econ. Geol.* **52,** 825–830.

Bear J. (1972) Dynamics of Fluids in Porous Media. Dover Publications, Inc.

Bethke C. M. and Brady P. V. (2000) How the Kd approach undermines ground water cleanup? *Ground Water* **38 (***3***),** 435–443.

Curti E. (1999) Coprecipitation of radionuclides with calcite: estimation of partitioning coefficients based on a review of laboratory investigations and geochemical data. *Appl. Geochem.* **14,** 433–445.

Doerner H. A. and Hoskins W. M. (1925) Co-precipitation of radium and barium sulfates. *J. Am. Chem. Soc.* **47,** 662–675.

Dove P. M. and Czank C. A. (1995) Crystal chemical controls on the dissolution kinetics of the isostructural sulfates; celestite, anglesite and barite. *Geochim. Cosmochim. Acta* **59,** 1907–1915.

Drever J. I. (1988) The Geochemistry of Natural Waters. Prentice-Hall.

Drever J. I. (1992) The Geochemistry of Natural Waters. 2nd Edition, Prentice-Hall.

EPA (1993) Diffuse NORM wastes: waste characterization and preliminary risk assessment. EPA.

Fisher R. S. (1995) Naturally occurring radioactive materials (NORM) in produced water and scale from Texas oil, gas and geothermal wells: geographic, geological and geothermal controls, pp. 43. The University of Texas at Austin.

Gautier J. M., Oelkers E. H., and Schott J. (2001) Are quartz dissolution rates proportional to B.E.T. surface areas? *Geochim. Cosmochim. Acta* **65 (***7***),** 1059–1070.

Glushko V. P., Medvedev V. A., Bergman G. A., Gurvich L. V., Yungman V. S., Alekseev V. I., Kolesov V. P., Vasil'ev B. P., Reznitskii L. A., Khodakovskii L., Vorob'ev A. F., Smirnova N. L., Gal'chenko G. L., Biryukov B. P. and Ioffe N. T. (1979) Thermal Constants of Compounds. *Acad. Sci., USSR.* **9(1)**.

Gray P. (1993) NORM contamination in the petroleum industry. *J. Petrol. Tech.* **45,** 12–16.

Hanor J. S. (2000) Barite-celestine geochemistry and environments of formation. In *Review in Mineralogy, Vol. 40 Sulfate Minerals* (ed. C. N. Alpers, J. L. Jambor, D. K. Nordstrom), pp. 193–276. Mineralogical Society of America.

Helfferich F. G. (1989) The theory of precipitation/dissolution waves. *AIChE J.* **35 (***1***),** 75–87.

Helgeson H. C., Delany J. M., Nesbitt H. W., and Bird D. K. (1978) Summary and critique of the thermodynamic properties of rock-forming minerals. *Am. J. Sci.* **278-A,** 1–221.

Holland H. D. (1956) The chemical composition of vein minerals and the nature of ore forming fluids. *Econ. Geol.* **51,** 781–797.

Huck P. M., McClymont G. L., Schwartz F. W., Nesbitt B. E., Anderson W. B., and Kratochvil B. (1989) Modelling of radium-226 leaching from barium-radium sulfate sludges. *Waste Man.* **9,** 157–163.

Kraemer T. F. and Reid D. F. (1984) Occurrence and behavior of radium in saline formation water in the U.S. Gulf coast region. *Iso. Geosci.* **2 (***2***),** 153–174.

Kulik D. A., Kersten M., Herser U., and Neumann T. (2000) Applications of. Gibbs energy minimization to model early-diagenetic solid solution aqueous-solution equilibria involving authigenic rhodochrosites in anoxic Baltic sea sediments. *Aqua. Geochem.* **6,** 147–199.

Langmuir D. (1997) Aqueous Environmental Geochemistry. Prentice Hall.

Langmuir D. and Riese A. C. (1985) The thermodynamic properties of radium. *Geochim. Cosmochim. Acta* **49,** 1593–1691.

Lasaga A. C. (1998) *Kinetic Theory in the Earth Sciences.* Princeton University Press.

Lawson R. T. (1985) The thermochemistry of radium. *Thermochim. Acta* **91,** 185–212.

Lindsay D. B. (1988) Radionuclides. In *Environmental Inorganic Chemistry—Properties, processes and estimation methods* (ed. L. Bodek, W. J. Lyman, W. F. Reehl and D. H. Rosenblatt), Chap. 9. Pergamon Press.

McIntire W. L. (1963) Trace element partition coefficients—A review and application to geology. *Geochim. Cosmochim. Acta* **27,** 1209–1264.

Morel F. M. M. (1983) *Principles of Aquatic Chemistry.* John Wiley and Sons.

Murphy W. M. and Helgeson H. C. (1988) Thermodynamics and kinetic constraints on reaction rates among minerals and aqueous solutions IV. Retrieval of rate constants and activation parameters for the hydrolysis constants for pyroxene, wollastonite, olivine, andalusite, quartz, and nepheline. *Am. J. Sci.* **289,** 17–101.

Murphy W. M. and Smith R. W. (1988) Irreversible dissolution of solid solutions: A kinetic and stoichiometryic model. *Radiochim. Acta* **44,** 395–401.

Nagra (1994) Technical Report 93–22. Nagra.

National Research Council (1999) Evaluation of guidelines for exposure to technologically enhanced naturally occurring radioactive materials. National Academy Press.

Nordstrom D. K., Plummer L. N., Langmuir D., Busenberg E., May H. M., Jones B. and Parkhurst D. L. (1990) Revised chemical equilibrium data for major water-mineral reactions and their limitations. In *Chemical Modeling of Aqueous Systems II* (ed. D. C. Melchior and R. L. Bassett), pp. 398–413.

Parkhurst D. L. (1995) User's guide to PHREEQC—A computer program for speciation, reaction-path, advective-transport and inverse geochemical modeling. *USGS, WRI.* 95–4227.

Parkhurst D. L. and Appello A. A. J. (1999) User's guide to PHREEQC (version 2)—A computer program for speciation, batch-reaction, one dimensional transport and inverse geochemical modeling. *USGS, WRI.* 99–4259.

Penn R. L., Zhu C., Xu H., and Veblen D. R. (2001) Iron oxide coatings on sand grains from the Atlantic coastal plain: HRTEM characterization. *Geol.* **29 (***9***),** 843–846.

Phillips S. L., Hale F. V., Silverster L. F. and Siegel M. D. (1988) Thermodynamic Tables for Nuclear Waste Isolation—Aqueous solution database. Lawrence Livermore Laboratory.

Plummer L. N. (1986) Approach to equilibrium in solid solution-aqueous solution systems: The KCl-KBr-H_2O systems at 25°C. In *Geochemical Processes at Mineral Surfaces*, pp. 561–573.

Rai D., Zachara J. M. and others. (1988) Chromium reactions in geologic materials. Battelle Pacific Northwest Laboratories, Electrical Power Research Institute.

Reardon E. J. (1981) Kd's-Can they be used to describe reversible ion sorption reactions in contaminant migration? *Ground Water* **19 (***3***),** 279–286.

Rimstidt J. D. and Barnes H. L. (1980) The kinetics of silica-water reactions. *Geochim. Cosmochim. Acta* **44,** 1683–1699.

Shock E. L. and Helgeson H. C. (1988) Calculation of the thermodynamic and transport properties of aqueous species at high pressures and temperatures: Correlation algorithms for ionic species. *Geochim. Cosmochim. Acta* **52,** 2009–2036.

Shock E. L., Sassani D. C., Willis M., and Sverjensky D. A. (1997) Inorganic species in geological fluids: Correlation among standard molal thermodynamic properties of aqueous cations, oxyanions, and acid oxyanions, oxyacids, and hydroxide complexes. *Geochim. Cosmochim. Acta* **61 (***5***),** 907–950.

Smith A. L. (1987) Radioactive-scale formation. *J. Petrol. Tech.* **39,** 697–706.

Sposito G. (1984) The Surface Chemistry of Soils. Oxford University Press.

Steefel C. I. and Van Capppellen P. (1990) A new approach to modeling water-rock interaction: The role of precursors, nucleation, and Ostwald ripening. *Geochim. Cosmochim. Acta* **54,** 2657–2677.

Stumm W. and Morgan J. (1981) Chemical Equilibria and Rates in Natural Waters. John Wiley & Sons.

Stumm W. and Morgan J. J. (1996) Aquatic Chemistry: An introduction emphasizing chemical equilibria in natural waters. John Wiley & Sons.

Sverjensky D. A. and Molling P. A. (1992) A linear free energy relationship for crystalline solids and aqueous ions. *Nature* **356,** 231–234.

Sverjensky D. A., Shock E. L., and Helgeson H. C. (1997) Prediction of the thermodynamic properties of aqueous metal complexes to 5 Kb and 1000°C. *Geochim. Cosmochim. Acta* **61,** 1359–1412.

Truesdell A. H. and Jones B. F. (1974) WATEQ, A computer program for calculating chemical equilibria of natural waters. *J. Res., USGS.* **2,** 233–274.

Walter A. L., Frind E. O., Blowes D. W., Ptacek C. J., and Molson J. W. (1994a) Modeling of multicomponent reactive transport in groundwater 1. Model development and evaluation. *Water Res. Res.* **30 (***11***),** 3137–3148.

Walter A. L., Frind E. O., Blowes D. W., Ptacek C. J., and Molson J. W. (1994b) Modeling of multicomponent reactive transport in groundwater 2. Metal mobility in aquifers impacted by acid mine tailings discharge. *Water Res. Res.* **30 (***11***),** 3149–3158.

White A. F. and Peterson M. L. (1990) Role of reactive-surface-area characterization in geochemical kinetic models. In *Chemical Modeling in Aqueous Systems II*, Vol. Am Chem. Soc. Symp. Series 416, pp. 461–475. American Chemical Society.

White G. J. (1992) Naturally occurring radioactive materials (NORM) in oil and gas industry equipment and wastes—a literature review, pp. 34. Department of Energy.

Wolery T. J. (1992) Eqn. 3/6, A software package for geochemical modeling of aqueous systems: Package overview and installation guide (version 7.0). Lawrence Livermore National Laboratory, USRL-MA-110661 PT1.

Yeh G. T. (1992) EQMOD: A chemical equilibrium model of complexation, adsorption, ion-exchange, precipitation/dissolution, oxidation-reduction and acid-base reactions. Department of Civil Engineering, The Pennsylvania State University.

Yeh G. T. and Tripathi V. S. (1989) A critical evaluation of recent development of hydrogeochemical transport models of reactive multi-components. *Water Res. Res.* **25 (***1***),** 93–108.

Yeh G. T. and Tripathi V. S. (1991) A model for simulating transport of reactive multispecies components: Model development and demonstration. *Water Res. Res.* **27 (***12***),** 3075–3094.

Zhu C. and Anderson G. M. (2002) Environmental Applications of Geochemical Modeling. Cambridge University Press.

Zhu C. and Burden D. S. (2001) Mineralogical compositions of aquifer matrix as necessary initial conditions in reactive contaminant transport models. *J. Contam. Hydrol.* **51 (***3–4***),** 145–161.

Zhu C., Hu F. Q., and Burden D. S. (2001) Multi-component reactive transport modeling of natural attenuation of an acid ground water plume at a uranium mill tailings site. *J. Contam. Hydrol.* **52 (***1–2***),** 85–108.

Zhu C., Xu H., Ilton E., Veblen D., Henry D., Tivey M. K., and Thompson G. (1994) TEM-AEM observations of high-Cl biotite and amphibole and possible petrological implications. *Am. Mineral.* **79,** 909–920.